Journal of Applied Fluid Mechanics, Vol. 16, No. 11, pp. 2082-2100, 2023.
Available online at www.jafmonline.net, ISSN 1735-3572, EISSN 1735-3645.
https://doi.org/10.47176/jafm.16.11.1845

Air Bubble Size and Its Transition in a Horizontal Tube Produced by Venturi-Nozzle Bubble Generator

W. H. Goo[1], P. B. Ganesan[1,2†], K. W. Yong[1], M. Y. Ahmad[3], Y. H. Yau[1] and F. Hamad[4]

[1] *Department of Mechanical Engineering, Faculty of Engineering, Universiti Malaya, 50603, Kuala Lumpur, Malaysia*
[2] *Centre for Energy Sciences & Centre for Research in Biotechnology for Agriculture (CEBAR), Universiti Malaya, 50603 Kuala Lumpur, Malaysia*
[3] *Department of Biomedical Engineering, Faculty of Engineering, Universiti Malaya, 50603, Kuala Lumpur, Malaysia*
[4] *Department of Mechanical Engineering, Teesside University Middlesbrough, Middlesbrough TS1 3BX, UK*

†*Corresponding Author Email: poo_ganesan@um.edu.my*

ABSTRACT

This paper investigates the air bubble size and its transition in a horizontal tube of 700 mm. The tube was assembled with a venturi-nozzle bubble generator. Air and water flow-rates vary in the present study. The data collection mainly used high-speed camera to capture the bubbles at different distances along the horizontal tube at water flow-rates (Q_w) of 120-170 litre per min (LPM) and air flow-rates (Q_a) of 2-10 LPM. MATLAB was used in image processing for evaluating the bubble size. The data interpretation used Y_W dimensionless parameter in representing the height of the bubbles' vertical rise in the horizontal tube. The bubble size along the horizontal tube was characterized by the Weber number as well. The type of two-phase (water-air bubbles) flow along the horizontal tube from the venturi-nozzle bubble generator was determined using flow pattern map and Lockhart-Martinelli parameter. The bubble generator produced bubbles in the range of 0.8-3.1 mm at the inlet of horizontal tube. The bubble diameters increased as the bubbles moved horizontally from inlet to outlet of the horizontal tube and this finding was statistically significant. The vertical rise height of bubbles along the horizontal tube at different water and air flow-rates had been quantified and compared. The vertical rise height of bubbles increased axially from 41 % to 89 % from inlet to outlet of the horizontal tube. The bubbles' vertical rise height increased when either the air flow-rate or water flow-rate is reduced. The mean Weber number increased along the horizontal tube due to an increase in bubble size. The decrease in water flow-rate caused a decrease in the mean Weber number. The Lockhart-Martinelli parameter of the water-air bubbles flow in the horizontal tube was within 0.58-2.94, indicating that it was a multiphase flow. The findings from this study give fundamental insight into bubble dynamics behaviour in its horizontal transition. This study focuses on the size and transition of air bubbles produced by venturi-nozzle bubble generator along a horizontal tube at different water and air flow-rates, unlike previous studies which only investigate the air bubbles inside or near bubble generator. These findings are very useful for practical industrial applications because the exact air bubble size before being used is known.

Article History

Received February 27, 2023
Revised June 9, 2023
Accepted June 29, 2023
Available online September 3, 2023

Keywords:

Horizontal flow
Flow visualization
Image processing
Statistical analysis
Bubble size
Inlet water flow-rate
Inlet air flow-rate

1. INTRODUCTION

Aeration is defined as the process of circulating, mixing or dissolving air or oxygen in a liquid or substance, i.e. water. Aeration is widely used in various engineering applications, such as aquaculture (Boyd, 1998; Roy et al., 2021) and wastewater treatment (Terasaka et al., 2011; Zhang et al., 2016). Water aeration is used in wastewater treatment to accelerate the removal of contaminants through aerobic digestion by increasing the dissolved oxygen concentration. Venturi-type bubble generator nozzle is a popular engineering tool for aeration applications. Venturi-type bubble generator contains hydraulic structures which can improve dissolved oxygen concentration significantly by creating turbulent

NOMENCLATURE

Q_w	volumetric flow-rate of water (LPM)	D_m	mean equivalent diameter of 10 air bubbles
Q_a	volumetric flow-rate of air (LPM)	V_a	velocity of air bubbles in horizontal tube
A	area of air bubble (m^2)	Q_l	volumetric flow-rate of liquid
D	equivalent diameter of air bubble (mm)	Q_g	volumetric flow-rate of gas
d_1	major diameter of air bubble (pixel)	v_{SL}	velocity of superficial liquid
d_2	minor diameter of air bubble (pixel)	v_{SG}	velocity of superficial gas
Y_W	dimensionless vertical rise height of air bubbles		
H_B	vertical height of air bubbles measured from top outer surface of horizontal tube (mm)	π	value of pi
OD_{ts}	outer diameter of test section	α	aspect ratio of air bubble
p	probability that the null hypothesis is true	χ	Lockhart-Martinelli parameter
F	F-value	ρ_w	density of water
F_c	Critical F-value	σ	surface tension of water-air interface
We	Weber number	ρ_g	density of gas
We_m	mean Weber number	ρ_l	density of liquid
V_w	velocity of water in horizontal tube		

conditions where air bubbles are carried into the bulk of the liquid flow (Baylar & Ozkan, 2006). Venturi-type bubble generator can easily modify the pressure and velocity of fluid passing through the constriction of its venturi structure. Venturi-type bubble generator has broad applications in engineering and research fields due to the benefits of low power consumption, simple and robust design, high bubble foaming efficiency, and high reliability. Many studies have been conducted to investigate the performance of venturi-type bubble generators with different structural designs. The most significant performance parameters for a venturi-type bubble generator are the bubble size and distribution (Huang et al., 2020). Venturi-type bubble generators can commonly be categorized into bubble generators or microbubble generators based on the size of the bubbles generated.

Past literature indicates that the bubble generation efficiency is influenced by the structural parameter of the bubble generator and the operating conditions. Different structural designs of bubble generators have been reported in past literature. Sadatomi et al. (2005) invented a novel microbubble generator with a spherical body installed in the centre of a flowing water tube to generate strong turbulence flow for the breakup of large bubbles into microbubbles. The air is entrained into the flowing water tube downstream from the body centre through drilled holes due to lower pressure. Sadatomi et al. (2012) then optimized the device into an orifice-type microbubble generator which contains an orifice and porous pipe instead of the spherical body and drilled holes in a flowing water tube. They found that the average microbubble size is further reduced using this design. However, these two designs display higher energy consumption and lesser throughput, which is not practical for most engineering applications. Besides, the flow path in the flowing water tube is also easily obstructed due to the existence of internal structures. Kurata et al. (2007) designed a compact microbubble generator to apply microbubbles into cell culture. 66.8 % of the bubbles produced by the device are within bubble diameter of 5-20 μm. Terasaka et al. (2011) compared the performance of four different microbubble generators, which are spiral liquid flow type, venturi type, ejector type, and pressurized dissolution type and three different gas distributors, which are constant flow nozzle plate, porous plate, and perforated plate for wastewater treatment. They found that the microbubble generators displayed higher oxygen transfer coefficients due to the smaller bubble size produced, especially so for the spiral liquid flow type microbubble generator compared to the gas distributors. However, the energy consumption of the microbubble generators is higher than the gas distributors. Zhao et al. (2018) fabricated a venturi channel with a rectangular cross-section. The rectangular cross-section is designed for better observation of individual bubble motion. They found that the deceleration of bubbles in the divergence section increases with the increase of liquid flow-rate. This is believed to play an important role in bubble breakup. Murai et al. (2021) also concluded that the rapid bubble deceleration, which causes bubbles' slip-back due to positive pressure gradient in the divergence section of a venturi-type microbubble generator under subsonic conditions (to prevent pressure shock waves) is the main reason for bubble fragmentation.

Wang et al. (2021) designed a novel swirl-venturi microbubble generator with four tangential inlets and studied the bubble breakup. They found that there are two additional bubble breakup patterns, i.e. static erosive breakup and dynamic breakup, other than tensile breakup in swirl-venturi microbubble generator compared to a conventional venturi microbubble generator. The swirl-venturi microbubble generator can generate daughter bubbles with smaller diameter and narrower distribution compared to the conventional venturi microbubble generator under the same experimental conditions. Ding et al. (2021) designed a new venturi bubble generator consisting of two serial rectangular venturi channels with the same geometrical dimension. It is found that the Sauter mean diameter of microbubble exiting the second outlet is smaller than the first outlet, but the difference is minimized by increasing the Reynolds number at the throat section.

Yun & Kim (2014) conducted computational fluid dynamics (CFD) simulations to investigate the effects of air supply hole size, position of holes, and number of holes on the air flow characteristics in a venturi tube. They found that the most optimum hole position is at the starting

point of diverging section due to the wide air suction angle. They also found that air entrainment increases linearly with the number of air supply holes and diameter of air supply hole. Yin et al. (2015) conducted experiments to prove that the volume-averaged bubble diameter has a power of -1 dependence on the Reynolds number and a linear relation with the gas volume ratio. Gordiychuk et al. (2016) studied the effects of different parameters, such as air flow-rate, water flow-rate, and air inlet size on the size distribution of microbubbles for a venturi-type microbubble generator. They concluded that bubble size is inversely proportional to the water flow-rate. Besides, they also found that the bubble size increases with the increase in the air/water ratio. Li et al. (2017) studied the effects of three different geometric parameters of a venturi-type bubble generator, i.e. injection hole diameter, injection hole number, and divergent angle, on the bubble size distribution. They proved that only divergent angle is sensitive to the bubble size distribution, whereas injection hole diameter and injection hole number has little effect on the bubble size distribution. Zhao et al. (2019) investigated the bubble motion and bubble breakup process in rectangular venturi channels with divergent angles of 7.5 °, 10 °, and 12.5 ° using Digital Image Analysis method. They found that the larger the divergent angle, the higher the maximum magnitude of bubble deceleration, the larger the bubble deformation rate, and the shorter the distance and time required for the bubble to decelerate. However, the modification of divergent angle does not affect the bubble breakup mechanism.

Wang et al. (2020) compared the performance of a swirl-venturi microbubble generator (SVMG) with 4 tangential inlets against a conventional venturi microbubble generator (VMG) experimentally. They found that the Sauter mean bubble size of both microbubble generators decreases with the increase in liquid velocity or decrease in air velocity, with SVMG showing smaller Sauter mean bubble size and narrower bubble size distribution than VMG. Sakamatapan et al. (2021) investigated the effects of water flow-rate on the number and size of microbubbles in a venturi-type bubble generator with equal entry and exit angles of 30 °. They concluded that the air flow-rate and number of air bubbles increase, whereas the size of microbubbles decreases when the water flow-rate increases. Lee et al. (2021) found that the average bubble diameter in a venturi-type microbubble generator decreases with the increase in exit angle. However, the average bubble diameter increases after exit angle of 15 ° due to the formation of wake region. The authors then designed different flared diffusers with an exit angle of 15 ° but different angular gradient to cause rapid flow changes while preventing wake formation and concluded that design F2 and F3 can produce smaller bubbles compared to design F3 (wake flow) and F4 (interaction with the central flow is relatively small due to relatively gentle angular gradient). Huang et al. (2021) found that decreasing the throat size of a venturi-type bubble generator causes the vortex regions to move upstream of the divergence section, which is beneficial for generating smaller bubbles due to the bubble deformation and breakup phenomenon being more intense. Wilson et al. (2021) found that the water flow-rate has the most significant effect on the size of the microbubbles produced by venturi-type microbubble generator compared to throat length/throat diameter ratio and divergent angle at water flow-rate of 8.21-13.3 LPM and air flow-rate that gives volumetric qualities of 0.05, 0.1, and 0.2. Lastly, Ding et al. (2022) concluded that the bubble breakup ratio in a venturi-type microbubble generator shows a first-order linear function relationship with the pressure drop, a Sine model fitting relationship with the angle ratio, and a Boltzmann function relationship with the throat length-diameter ratio.

A comparison of geometrical dimensions for this venturi-nozzle bubble generator with other literature is tabulated in Table 1. The literature compared are from the year 2015 to 2022 and is related to venturi-nozzle bubble generators. The bubble generators from most literature have conventional water inlets with cross-sectional areas that are either circular or rectangular-shaped, except for Wang et al. (2020) and Wang et al. (2021) who used 4 tangential inlets to induce swirling flow in their bubble generators. The air inlets of the bubble generators from past literature mostly consist of several circular holes in the throat section. The convergence and divergence angles of the bubble generators from past literature are within 5.7-30 ° and 3.75-30 °, respectively.

A comparison of experimental parameters, such as the water flow-rate (Q_w) and air flow-rate (Q_a) during experiments, air inlet, bubble measurement, and the size of bubbles produced with those of other literature is tabulated in Table 2. The range of Q_w and Q_a studied by the past researchers is within 0.005-343.33 LPM and 0-8.25 LPM, respectively. Only Sakamatapan et al. (2021) presented venturi-nozzle bubble generator with passive air suction (vacuum), whereas most of the other studies presented bubble generators with active air suction (air compressor or peristaltic pump). For the evaluation of bubble size, most past literature evaluated the bubble size directly in the throat or divergence section of bubble generator. Past researchers such as Yin et al. (2015), Li et al. (2017), Sun et al. (2017), Sakamatapan et al. (2021), and Levitsky et al. (2022) evaluated the bubble size in a test section located away from the bubble generator. The diameters of bubbles generated by the venturi-nozzle bubble generator from past studies are within the range of 0-4.2 mm.

The novelty of the venturi-nozzle bubble generator design from this study is the shape and location of the air inlet. This bubble generator design has a ring-shaped air inlet located along the entire divergence section which, to the best of our knowledge, is not found in the past literature. This bubble generator design was based on two pipe connectors and was initially applied for water aeration of 7,000-10,000 litres of water in a fish tank using a high-pressure pump (0.75 kW) for aquaculture application. Just by comparing the geometrical dimensions of water inlet, outlet, and throat, the size of this bubble generator is considerably larger than most bubble generators found in the past literature. Besides, the convergence and divergence angles of this bubble generator are 39.84 ° and 27.92 °, respectively, which are the largest angles (except for the bubble generator of

Table 1 Comparison of geometrical dimensions for venturi-nozzle bubble generator with other literature

Reference	Hydraulic Diameter of Water Inlet (mm)	Diameter of Air Inlet (mm)	Location of Air Inlet	Hydraulic Diameter of Outlet (mm)	Length of Convergence Section (mm)	Length of Divergence Section (mm)	Hydraulic Diameter of Throat (mm)	Length of Throat (mm)	Convergence Angle (°)	Divergence Angle (°)
Our Study (2023)	48.2	5.66 (Ring)	Divergence Section	26.8	16	5	21.5	28	39.84	27.92
Levitsky et al. (2022)	-	0.3 (2 Holes per Bush)	Throat	-	-	-	6	-	30	25
Huang et al. (2019)	1.5 / 1.6	1 (1 Hole)	Throat	-	-	-	1 - 0.67	24 - 20	22.5	7.5
Zhao et al. (2017)	50	1.5 (12 Holes)	Throat	50	-	-	25	-	22.5	7.5
Zhao et al. (2018)	16.67	1 (1 Hole)	Throat	16.67	-	-	14.29	-	22.5	7.5
Ding et al. (2021)	8.33	1 (1 Hole)	Water Inlet	8.33	-	-	8.33	15	22.5	10
Huang et al. (2020)	1.6	1 (1 Hole)	Throat	-	-	-	1.9	20	22.5	7.5
Wang et al. (2021)	6 (4 Tangential Inlets)	6 (1 Hole)	Throat	26	40	40	18	0	5.7	5.7
Sun et al. (2017)	50	1.5 (12 Holes)	Throat	50	-	-	25	-	22.5	7.5
Zhao et al. (2019)	16.67	1 (1 Hole)	Throat	16.67	-	-	14.29	55	22.5	3.75 - 6.25
Sakamatapan et al. (2021)	66	2 (1 Hole)	Throat	51.4	-	-	30	10	30	30
Song et al. (2019)	53	1 (1 Hole)	Throat	-	37	113	23	50	22.5	7.5
Yin et al. (2015)	53	1 (4 Holes)	Throat	53	114	36	23	50	8	-
Li et al. (2017)	-	1 - 3 (1 - 4 Holes)	Throat	53	47	-	23	50	22.5	7.5 - 12.5
Wang et al. (2020)	6 (4 Tangential Inlets)	6 (1 Hole)	Throat	26	40	40	18	0	-	18
Huang et al. (2018)	16.67	1 (1 Hole)	Throat	-	-	-	14.29	55	22.5	3.75 - 6.25

Sakamatapan et al. (2021) with a divergence angle of 30 °), compared to past literature with convergence and divergence angles of mostly 22.5 and 7.5 °, respectively. The range of Q_w investigated in this study is only 120-170 LPM, which is lower compared to the past literature. However, the range of Q_a studied is 2-10 LPM, which is among the highest in comparison with the previous studies. The bubble generator in this study was studied using passive air suction. This is suitable for cost-saving purposes since only a water pump is needed for the bubble generator to function. However, experimental study of the bubble generator using passive air suction has limited the maximum Q_a achievable by the bubble generator. The bubble size and its transition were evaluated in a horizontal tube located away from the bubble generator. This poses an advantage for practical industrial applications since the exact bubble size before being used instead of inside the bubble generator is known. The distance of the horizontal tube from the bubble generator outlet in this study was 160 mm. The sizes of bubbles produced by this bubble generator were within 0.8-3.1 mm, which is among the largest compared to the previous studies, at the inlet of the horizontal tube. This is due to the occurrence of bubble coalescence before the bubbles enter the horizontal tube. The bubble size should be significantly reduced if the horizontal tube is placed nearer to the horizontal tube, or the bubble measurement is carried out inside the bubble generator.

Most of the previous studies, such as Yin et al. (2015), Sun et al. (2017), Zhao et al. (2018), Huang et al. (2020),

Table 2 Comparison of experimental parameters with other literature

Reference	Q_w (LPM)	Q_a (LPM)	Air Inlet	Bubble Size Measurement	Bubble Size (mm)
Our Study (2023)	120 - 175	2 - 10	Passive	Test Section	0.8 - 3.1 (Inlet of Test Section)
Levitsky et al. (2022)	0.83	0.075 - 0.3	-	Test Section	0 - 0.8
Huang et al. (2019)	2.1 - 10.2	0.02 - 0.13	Active	Bubble Generator	0 - 1.2
Zhao et al. (2017)	250 - 343.33	0.0033 - 0.02	Active	Bubble Generator	0.6 - 2.8
Zhao et al. (2018)	30 - 183.33	0.13 - 1.33	Active	Bubble Generator	1.2 - 4.2
Ding et al. (2021)	4.17 - 15	0.1 - 0.6	Active	Bubble Generator	0 - 3
Huang et al. (2020)	0.2 - 1.2	0.001 - 0.16	Active	Bubble Generator	0.2 - 0.4
Wang et al. (2021)	0.005-0.015	0.003	Active	Bubble Generator	0 - 0.2
Sun et al. (2017)	166.67 - 500	0 - 2	Active	Test Section	0.5 - 0.6
Zhao et al. (2019)	10 - 150	0.13 - 1.23	Active	Bubble Generator	0 - 1.6
Sakamatapan et al. (2021)	166.67 - 300	0.85 - 3.53	Passive	Test Section	0.05 - 0.26
Song et al. (2019)	66.67 - 183.33	100 rad/min (Peristaltic Pump)	Active	Bubble Generator	1.08 - 3.03
Yin et al. (2015)	116.67 - 316.67	0.12 - 2.53	Active	Test Section	0.3 - 1.4
Li et al. (2017)	83.33 - 333.33	0.08 - 1.68	Active	Test Section	0 - 1.5
Wang et al. (2020)	5 - 25	0.06 - 0.6	Active	Test Section	0 - 5
Huang et al. (2018)	31.67 - 150	0.07 - 8.25	Active	Bubble Generator	-

Note: Passive = Vacuum, Active = Air Compressor or Peristaltic Pump

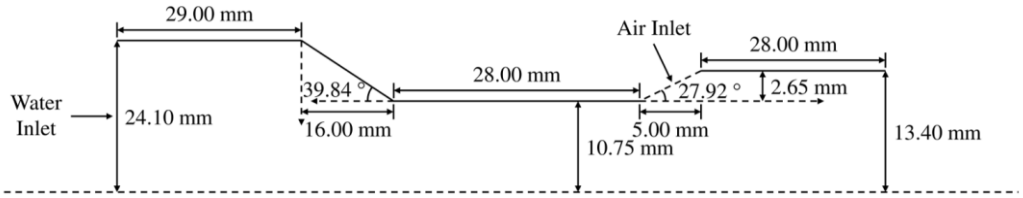

Fig. 1 2D dimensions of venturi-nozzle bubble generator

etc, are limited to the investigation and assessment of air bubble size and air bubble characteristics within or near any specific nozzle (bubble generator) area. In a real-life application, often the bubbles move from the nozzle towards other sections of water, and therefore it is important to understand the transition of bubble diameter as it moves horizontally. In an aquaculture application, which is the main motivation of this study, air bubbles are expected to move horizontally from the venturi-nozzle bubble generator to other sections of water in a culture tank to improve the dissolved oxygen concentration. Therefore, we have focused on the horizontal transition of air bubbles. The objectives of this study are to evaluate the air bubble size and study the size transition of air bubbles along a horizontal (axial) tube generated by an in-house designed venturi-nozzle bubble generator. The effects of Q_a and Q_w on the bubbles generated by the bubble generator were studied at 7 different positions in a horizontal tube experimentally. The flow of the bubbles was captured using high-speed camera, and then the images were post-processed using MATLAB to evaluate the bubble size. In addition, the effects of Q_a and Q_w on the vertical rise height of bubbles (Y_W) were also investigated. Statistical analysis was also conducted to verify the significance of the data obtained.

2. METHODOLOGY

2.1 Venturi-Nozzle Bubble Generator

The cross-section geometry of the bubble generator is shown in Fig. 1. The bubble generator is composed of three main sections: the convergence section, throat, and divergence section. The air inlet is located along the divergence section and has a ring-shaped geometry with a diameter of 5.66 mm. There is a pressure difference between the flowing water in the throat section of bubble generator and atmospheric air due to the venturi structure. Air is drawn into the bubble generator through the air inlet due to low (vacuum) pressure in the throat section where bubbles are formed and then break apart due to pressure recovery in the divergence section.

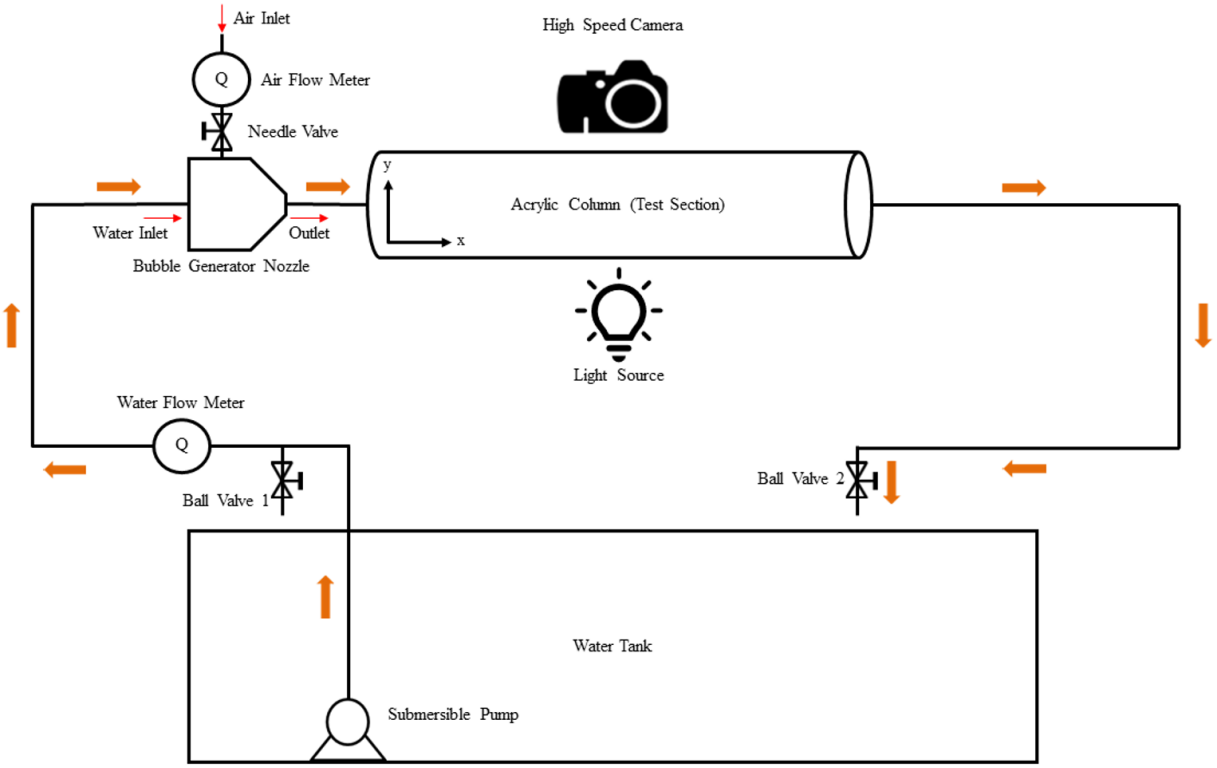

Fig. 2 Schematic drawing of experimental setup

2.2 Experimental Setup

Ambient air and tap water were used as the working fluids. The temperature and relative humidity of air were 30.7 °C and 72.8 %, respectively, whereas the water temperature was 27.8 °C. The schematic diagram of the experimental setup is shown in Fig. 2. A submersible pump (LEO XSP 9-7.5/0.25L, China) with an input power of 0.25 kW, head of 2.4-7.2 m, and can provide a constant 15-149 litres per minute (LPM) of water flow according to the technical specifications, was used to pump water from a water tank to the bubble generator. A water flow meter (YF-DN50, China), with a measurable Q_w range of 10-300 LPM and an accuracy of ±3 %, was used to measure the inlet Q_w to the bubble generator. An air flow meter (MF 5706, USA), with a measurable range of 0-10 LPM and an accuracy of ±2.5 %, was used to measure the Q_a into the bubble generator. The bubble images were recorded using high-speed camera (Phantom Miro M310, USA) at a shooting frame of 1,000 frames per second (fps) with a resolution of 1,280 x 800 pixels. A 100 W white LED flood light was used as the light source to increase the light contrast when capturing bubble images. The horizontal tube, which is the test section, is a transparent acrylic tube with an inner diameter, thickness, and length of 41 mm, 2 mm, and 700 mm, respectively, and it was used for the bubble flow visualization. Bubble images were captured at 7 different axial sections of the horizontal tube with lengths of 100 mm each. A reference scale was placed on top of the horizontal tube to calculate the pixel-to-mm image resolution.

2.3 Experimental Cases

In this study, the effects of the incoming Q_a and Q_w were investigated on bubble horizontal (axial) flow and its size transition. The results will be reported for seven axial positions (i.e., Position 1-7) after the flow is discharged from the bubble generator. The intended experimental cases are tabulated in Table 3. Basically, a total of 12 experimental cases were carried out in which Q_w varies from 120 LPM (namely as Case B), 145 LPM (namely as Case C), to 170 LPM (namely as Case D), with Q_a ranging from 2, 4, 6, 8 to 10 LPM. For each case, the bubble axial flow was captured for 7 different axial positions between 0-700 mm of the horizontal tube. The distance between the nozzle outlet and inlet of the horizontal tube (i.e., Position 1) was 160 mm. The maximum Q_a will be decreased if the Q_w is reduced due to the passive air suction nature of the bubble generator.

Table 3 Intended experimental cases

Number of Data Set	Case	Q_w (LPM)	Q_a (LPM)	Position
35	B	170	10 (B1), 8 (B2), 6 (B3), 4 (B4), 2 (B5)	1-7
28	C	145	8 (C1), 6 (C2), 4 (C3), 2 (C4)	1-7
21	D	120	6 (D1), 4 (D2), 2 (D3)	1-7

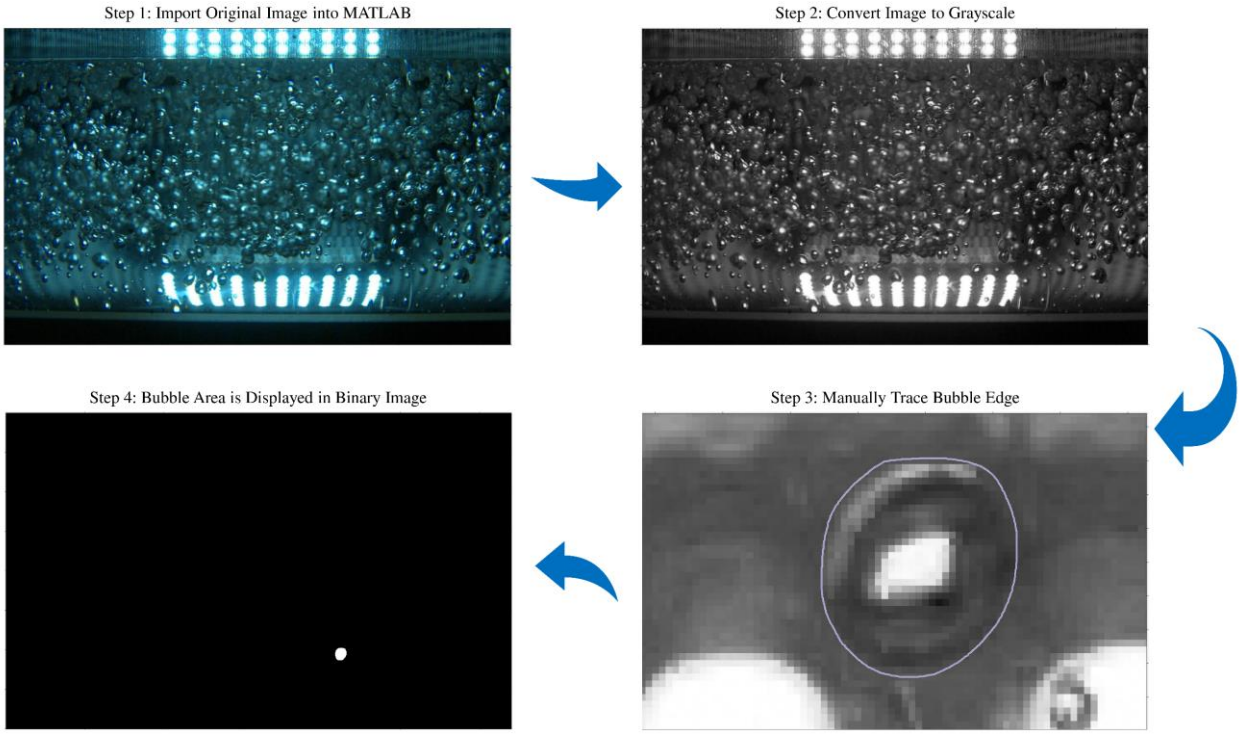

Fig. 3 Procedures to obtain bubble area in pixels

2.4 Evaluation of Air Bubble Size using Image Processing

Image processing techniques and methods by Sun et al. (2017) and Sakamatapan et al. (2021) have been used as references for the evaluation of the air bubble size. Briefly, there are four main procedures in obtaining the bubble area in pixels as shown in Fig. 3. They are; (i) Importing original image into MATLAB; (ii) Converting the imported image into grayscale; (iii) Tracing the bubble edge manually; (iv) Displaying the bubble area in binary image. First, the original bubble image was imported into MATLAB to be further processed. After that, the imported bubble image was converted into grayscale. In MATLAB, a gray image is represented as a matrix with each of its element corresponding to one pixel in the image (Zhao et al., 2018). Then, the bubble edge of individual bubbles was manually traced using an in-house developed algorithm. MATLAB built-in function "bwarea" was used to obtain the manually drawn bubble area in pixels whereas the "regionprops" function was used to obtain the major and minor axis length of the manually drawn bubble. Lastly, the manually drawn bubble area was displayed in binary image. The bubble area was converted from pixels to mm by obtaining the image resolution from a reference scale installed on top of the horizontal tube. The image resolution, which was highly dependent on the distance of the high-speed camera from the horizontal tube, was within 12-15 pixel length/mm. Since the bubble volume was not obtainable in this work, 2-dimensional (2-D) analysis was conducted to calculate the bubble size. In this study, the bubble size was defined by evaluating its equivalent diameter. On the other hand, the bubble shape was defined by the aspect ratio of the largest diameter to its smallest diameter. The bubble area is converted from pixels to mm using the image resolution. The equivalent diameter of air bubble (D) and aspect ratio of air bubble (α) are defined by Eq. (1) and Eq. (2), respectively.

$$D = 2\sqrt{\frac{A}{\pi}} \tag{1}$$

$$\alpha = \frac{d_1}{d_2} \tag{2}$$

Where A is the area of air bubble, d_1 is the major diameter of air bubble, and d_2 is the minor diameter of air bubble. The bubble equivalent diameter is approximated by assuming that the diameter of a 2-D bubble in an image is equal to a circular bubble with the same area (Zhao et al., 2017). The α is not lesser than 1, and the closer α to 1, the more circular the bubble is. For each image, 10 visually clear bubbles were selected to evaluate their equivalent diameters. The bubble images for each experimental case were recorded for 4.116 seconds at 1,000 fps due to the limitation of the high-speed camera. The image recording process for every case was repeated 0-3 times as necessary to ensure that the video quality was suitable for image processing. A single visually clear bubble image for every case was then extracted and used for image processing and evaluation of bubble size. Some steps were taken to ensure the measurement accuracy of the bubble size. For each bubble, the bubble area, major and minor diameters were captured by averaging three different measurements. In addition, the difference between each measurement for a specific bubble was set to be lesser than 30 pixels for bubble area and lesser than 3 pixels for bubble major diameter and bubble minor diameter, which produced a standard deviation of ≤ 0.042 mm and ≤ 0.1249 in bubble equivalent diameter and α, respectively. All calculations were conducted using Microsoft Excel.

2.5 Vertical Rise Height of Air Bubbles Along Horizontal Tube

The vertical rise height of bubbles for each case from inlet to outlet of the horizontal tube (i.e., Position 1 to 7) was measured manually from the original bubble images. The dimensionless number, Y_W which indicates the proportion of horizontal tube not occupied with air bubbles, is defined in Eq. (3).

$$Y_W = \frac{1-H_B}{OD_{ts}} \tag{3}$$

Where H_B is the vertical height of air bubbles measured from the top outer surface of horizontal tube and OD_{ts} is the outer diameter of the test section (horizontal tube), which is 45 mm. For example, Y_W of 0 means that the whole horizontal tube is occupied with bubbles whereas Y_W of 0.8 means that only 20 % of the horizontal tube is occupied with bubbles. The effects of Q_a and Q_w on Y_W were plotted using bar graphs. For the evaluation of H_B from Eq. (3), the vertical height from the top outer surface of the horizontal tube to the level where there is almost no bubble was first measured using a ruler. The height measured by the ruler was then converted to the actual height (H_B) using the outer diameter of the horizontal tube, OD_{ts} as a reference, which is 45 mm.

2.6 Statistical Analysis

One-way ANOVA of variance which depended on the p-value (Prob. > F) at the 0.1 % confidence interval, was applied in this study to compare the bubble equivalent diameters (Liu et al., 2019). The model determines the statistical significance of the ratio of the mean square variation due to regression and the mean square residue error (Verma et al., 2015). The p-value is defined as the probability of seeing the observed F value if the null hypothesis is true without any factor effect (Liu et al., 2019). Basically, the statistical analysis for comparisons of treatment means was carried out with $p < 0.001$. If $F > F_c$, this indicates that there is at least 1 difference between the means of the data groups, and it can be concluded that the data obtained for the specific data groups are statistically significant. Conversely, if $F < F_c$, this indicates that there is no difference between the means of the data groups, and it can be concluded that the data obtained for the specific data groups are statistically insignificant. The means of overall equivalent diameter for all cases were reported with appropriate standard deviations (±standard deviation) and are tabulated in Table 4-6. The results related to bubble diameters were presented in box plots as shown in Fig. 4-5 and Fig. 9-10. In addition, the α from inlet to outlet of the horizontal tube (i.e., Position 1 to 7) for Case B3 and Case C2 were presented in box plots as well, as shown in Fig. 6 and Fig. 11, respectively.

3. RESULTS AND DISCUSSION

3.1 The Effects of Q_a

The diameters of bubbles for Q_a of 2-10 LPM at constant Q_w of 170 LPM are presented in box plots, see Fig. 4. By comparing the bubble diameters at Q_a of 2-10 LPM from inlet to outlet of the horizontal tube (i.e., Position 1 to 7), the changes in bubble diameters with varying Q_a at all axial positions are minimal and insignificant. Now compare the bubble sizes between Position 1-4 (near inlet) and Position 5-7 (near outlet). The standard deviations of bubble diameters at Position 1-4 are smaller in comparison with that of Position 5-7. For example, referring to Fig. 4a and Fig. 4e, the distribution of bubble diameters at Position 1 is smaller compared to Position 5. This is because the tendency of bubble coalescence at Position 5 is higher compared to Position 1 as the bubbles are located nearer to the outlet of horizontal tube.

The overall bubble diameters for varying Q_a are tabulated in Table 4. The asterisk symbols within the p-value column indicate that the changes in bubble diameters with different Q_a are statistically significant ($p < 0.001$). There are a total of 21 data sets with 30-50 data taken for each set (10 bubbles for each Q_a). The overall bubble diameters increase axially from inlet to outlet of the horizontal tube (i.e., Position 1 to 7) at constant Q_w of 170 LPM, 145 LPM, and 120 LPM. The standard deviations of overall bubble diameters at Position 1-4 are also lower than that of Position 5-7, which coincide with the results from Fig. 4. For example, referring to Position 1 and Position 5 at Q_w of 170 LPM, the overall bubble diameter at Position 1 is 1.475±0.284 mm, in which the standard deviation is smaller than Position 5 with an overall diameter of 3.178±0.659 mm. However, statistical analyses show that 17 out of 21 data sets collected have $p > 0.001$, which indicates that Q_a is not a significant factor that affects bubble size. A similar finding is also obtained from Fig. 4.

The bubble diameters from inlet to outlet of the horizontal tube (i.e., Position 1 to 7) at constant Q_w of 170 LPM are presented in box plots, see Fig. 5. The bubble diameters increase with the axial distance from Position 1-7; The increase appears to be linear with the axial position. This finding implies that the bubbles undergo a coalescence process and therefore result in the increase of bubble sizes as they move axially. Now compare the bubble sizes at Position 1-4 (near inlet) and Position 5-7 (near outlet). The standard deviations of bubble diameters at Position 1-4 are smaller in comparison with that of Position 5-7, which coincide with the findings from Fig. 4. The diameters of bubbles from Position 1-7 are within 0.8-5.5 mm at 120 LPM$\leqslant Q_w \leqslant$170 LPM and 2 LPM$\leqslant Q_a \leqslant$10 LPM. The bubble diameters are within 0.8-3.1 mm at Position 1 only.

The overall bubble diameters from inlet to outlet of the horizontal tube (i.e., Position 1 to 7) are tabulated in Table 5. The asterisk symbols within the p-value column indicate that the changes in bubble diameters from Position 1-7 are statistically significant ($p < 0.001$). The last column tabulates the results of vertical rise height of bubbles (Y_W) for each case, which will be discussed later. By referring to the Q_a and Q_w columns, the actual Q_a and Q_w values for each case differ from the intended experimental cases tabulated in Table 3, with Q_w deviating more from the intended values compared to Q_a. This is because the Q_w and Q_a were manually controlled using a ball valve and needle valve, respectively during the

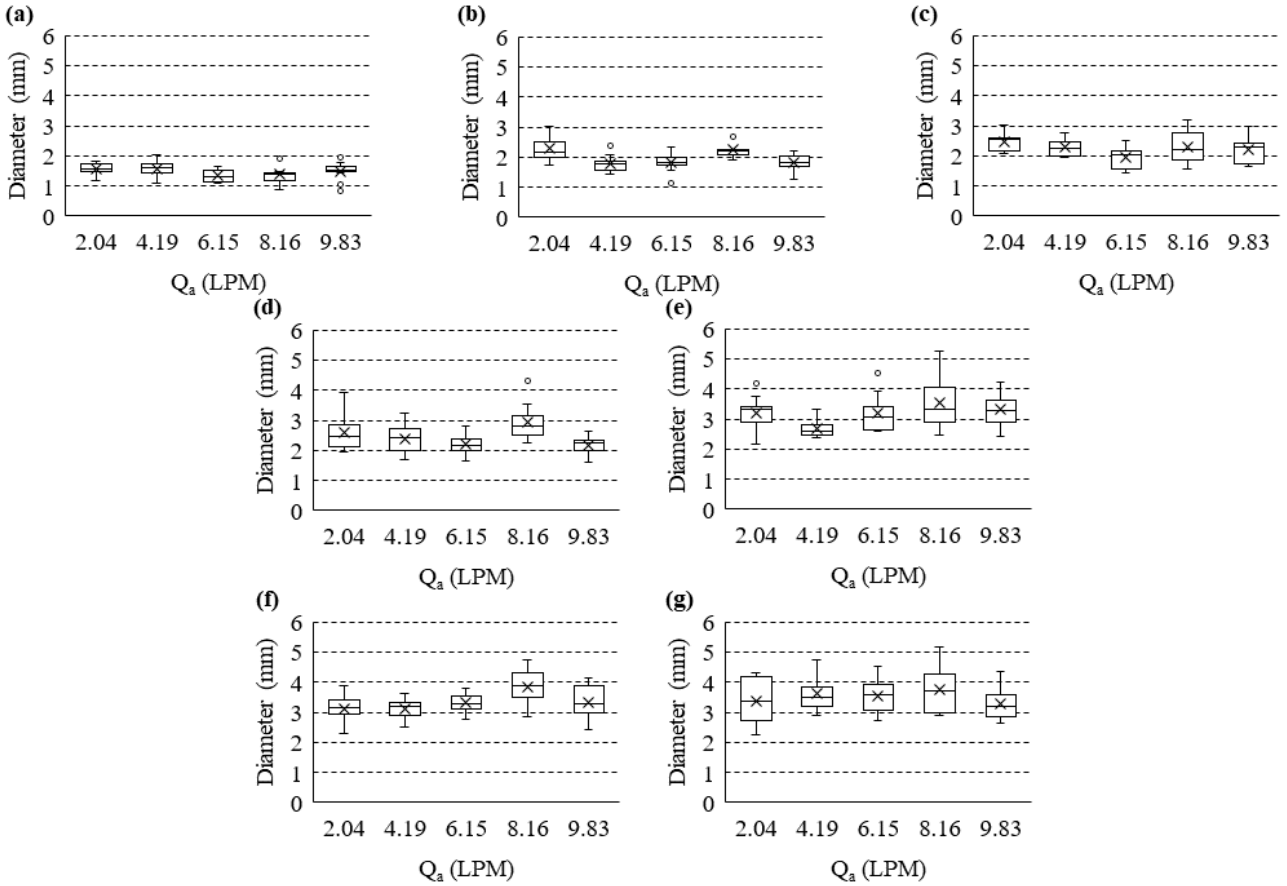

Fig. 4 Diameters of 10 bubbles at Position (a) 1, (b) 2, (c) 3, (d) 4, (e) 5, (f) 6, and (g) 7, for different Q_a at Q_w of 170 LPM

Table 3 Overall diameter of bubbles at different Q_a

Q_w (LPM)	Q_a (LPM)	Position	Overall Diameter (mm)	P-Value
170 LPM (170.62±3.81 LPM)	Case B1 (9.83±0.60 LPM), Case B2 (8.16±0.35 LPM), Case B3 (6.15±0.26 LPM), Case B4 (4.19±0.01 LPM), Case B5 (2.04±0.01 LPM)	1	1.475±0.284	> 0.001
		2	1.991±0.389	< 0.001*
		3	2.228±0.427	> 0.001
		4	2.459±0.565	> 0.001
		5	3.178±0.659	> 0.001
		6	3.34±0.549	> 0.001
		7	3.517±0.683	> 0.001
145 LPM (145.60±3.68 LPM)	Case C1 (8.27±0.51 LPM), Case C2 (6.03±0.32 LPM), Case C3 (4.08±0.21 LPM), Case C4 (2.01±0.06 LPM)	1	1.643±0.367	> 0.001
		2	2.344±0.418	> 0.001
		3	2.928±0.574	< 0.001*
		4	3.346±0.66	< 0.001*
		5	3.588±0.546	> 0.001
		6	3.606±0.663	> 0.001
		7	3.737±0.712	> 0.001
120 LPM (121.39±3.33 LPM)	Case D1 (5.89±0.59 LPM), Case D2 (4.19±0.23 LPM), Case D3 (2.02±0.08 LPM)	1	2.126±0.355	> 0.001
		2	2.689±0.331	> 0.001
		3	3.208±0.724	< 0.001*
		4	3.347±0.569	> 0.001
		5	3.44±0.637	> 0.001
		6	3.772±0.907	> 0.001
		7	3.813±0.809	> 0.001

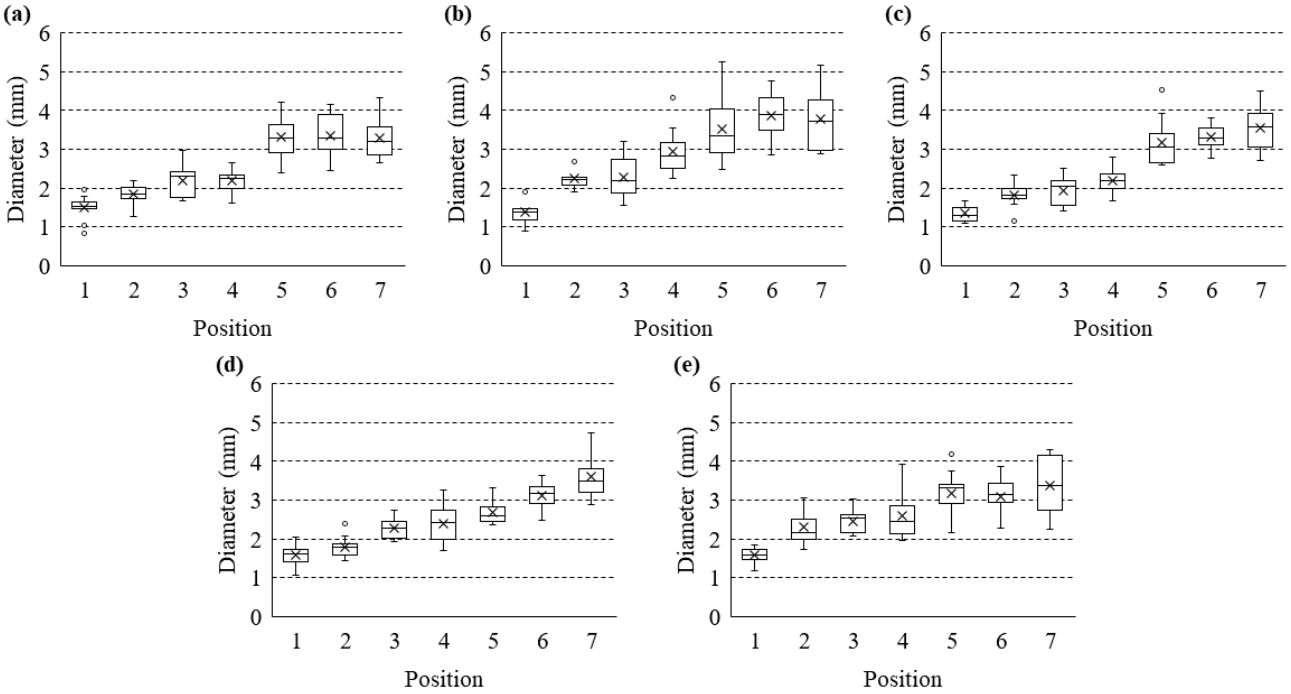

Fig. 5 Diameters of 10 bubbles at Q_w of 170 LPM with Q_a of (a) 10 LPM, (b) 8 LPM, (c) 6 LPM, (d) 4 LPM, and (e) 2 LPM

Table 4 Overall diameter of bubbles at Position 1-7

Case	Q_w (LPM)	Q_a (LPM)	Overall Diameter (mm)	P-Value	Increase in Bubble Size (%)	Y_W (H_B/OD_{ts})
B1	167.24±1.83	9.83±0.60	2.517±0.854	< 0.001*	120.31	0→0.41
B2	168.28±2.23	8.16±0.35	2.855±1.044	< 0.001*	170.64	0→0.52
B3	169.05±1.76	6.15±0.26	2.475±0.904	< 0.001*	164.54	0→0.52
B4	172.21±2.43	4.19±0.01	2.493±0.770	< 0.001*	129.94	0→0.52
B5	175.92±2.44	2.04±0.01	2.650±0.769	< 0.001*	113.58	0→0.58
C1	143.33±2.58	8.27±0.51	3.137±1.011	< 0.001*	151.84	0→0.69
C2	143.46±2.04	6.03±0.32	3.381±0.958	< 0.001*	115.75	0→0.71
C3	145.32±2.24	4.08±0.21	2.929±0.829	< 0.001*	138.39	0→0.72
C4	150.47±2.44	2.01±0.06	2.662±0.718	< 0.001*	107.24	0→0.72
D1	118.66±1.69	5.89±0.59	3.275±0.884	< 0.001*	67.55	0→0.78
D2	120.33±1.51	4.19±0.23	3.439±0.842	< 0.001*	85.45	0→0.89
D3	125.37±1.90	2.02±0.08	2.885±0.740	< 0.001*	86.51	0→0.89

experiments. A needle valve has much more flexibility in flow control applications whereas a ball valve is mostly used for on-off operation. There are a total of 12 cases with 70 data taken for each case (10 bubbles for each position). By referring to the overall diameter column, the overall bubble diameters from Position 1-7 appears to be smaller for lower Q_a. Past literature has shown that the bubble diameter decreases with decreasing Q_a (Sadatomi et al., 2005, 2012; Sun et al., 2017; Wang et al., 2020). Note that the bubble size was evaluated directly in either the throat or divergence section of bubble generator in most past literature, whereas the bubble size was evaluated along a

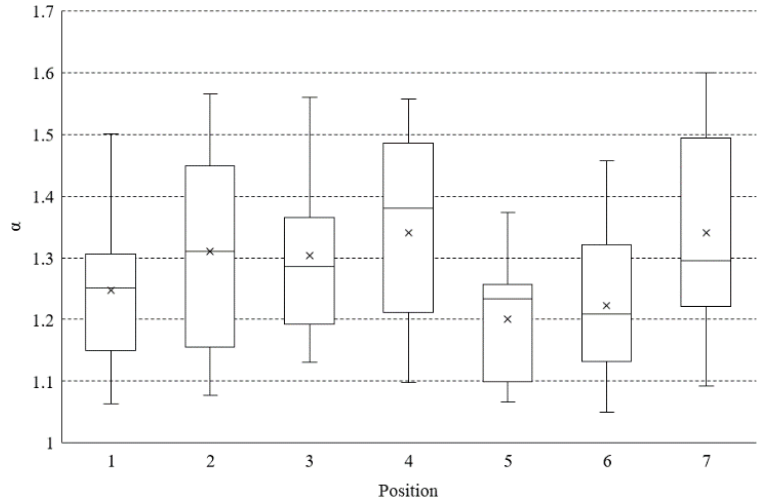

Fig. 6 Aspect ratios of 10 bubbles at Q_w of 170 LPM with Q_a of 6 LPM

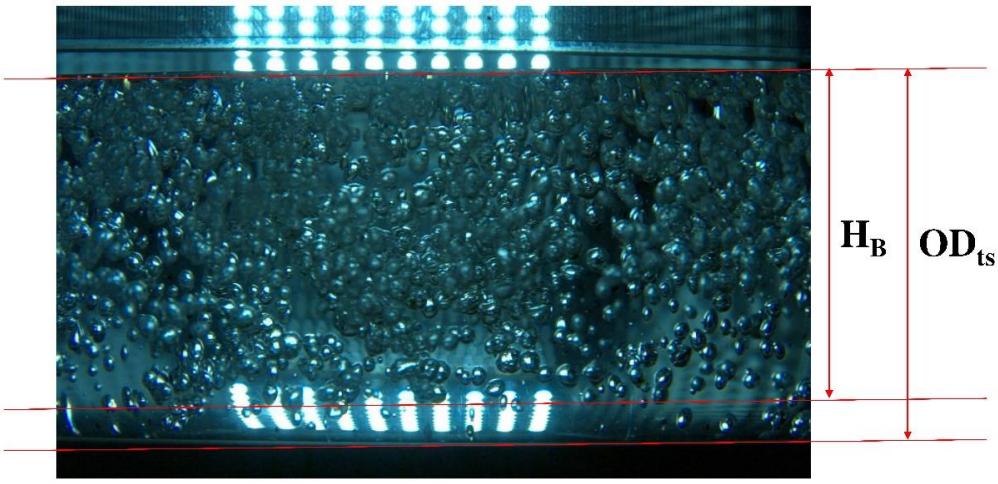

Fig. 7 Bubble image for Q_w of 170 LPM and Q_a of 10 LPM (Case B1) at Position 4

horizontal tube located 160 mm away from the bubble generator outlet in this study. The changes in bubble diameters from Position 1-7 for every case are statistically significant ($p < 0.001$). The increase in bubble diameters from Position 1-7 is within 67.55–170.64 %; The increase seems to be larger for higher Q_a at Q_w of 170 LPM and 145 LPM. This is due to the increase in bubble velocity in the horizontal tube as Q_a increases, which increases the tendency of bubble coalescence. However, a reverse trend is obtained for Q_w of 120 LPM. This could be due to some uncontrollable external factors during the experiments. The aspect ratios of bubbles from inlet to outlet of the horizontal tube (i.e., Position 1 to 7) at Q_w of 170 LPM with Q_a of 6 LPM are presented in a box plot, see Fig. 6. The α varies within 1-1.6. There is no significant change in α with the axial position, which has been validated by statistical analysis ($p > 0.001$).

An example of bubble image captured by the high-speed camera at Position 4 (i.e., around middle of the horizontal tube) for Case B1 is shown in Fig. 7. The red lines represent the H_B and OD_{ts} for the evaluation of Y_W. The Y_W from inlet to outlet of the horizontal tube (i.e., Position 1 to 7) at constant Q_w of 170 LPM, 145 LPM, and 120 LPM are presented in bar graphs, see Fig. 8. First of all, it is easily observed from Fig. 7 that the bubbles are not spherical-shaped due to bubble coalescence. The coalescence process of individual bubbles could not be observed and explained properly due to the bubbles being too densely packed together. However, the aspect ratios of bubbles along the horizontal tube at Q_w of 170 LPM and Q_a of 6 LPM (Case B3) have been plotted in a box plot, see Fig. 6; See Fig. 11 in Section 3.2 for the α along the horizontal tube at Q_a of 6 LPM and Q_w of 145 LPM (Case C2). It is clearly observed that the Y_W increases with the axial position. This finding can be used to explain the results from Fig. 5 and Table 4. The bubble diameters increase with the axial position because the bubbles travel upwards to the top of horizontal tube axially from Position 1-7, thus increasing the tendency of bubble coalescence. By referring to the Y_W at Q_w of 170 LPM, the Y_W increases with decreasing Q_a from 10-2 LPM. The same trend is observed for Q_w of 145 LPM and 120 LPM as well. This is because the velocity of bubbles reduces. Therefore, the bubbles have more time to travel to the top of horizontal tube when the Q_a is reduced, thus reducing H_B, which increases Y_W. Now refer to Table 5. The last column tabulates the increase of Y_W from Position 1-7 for each

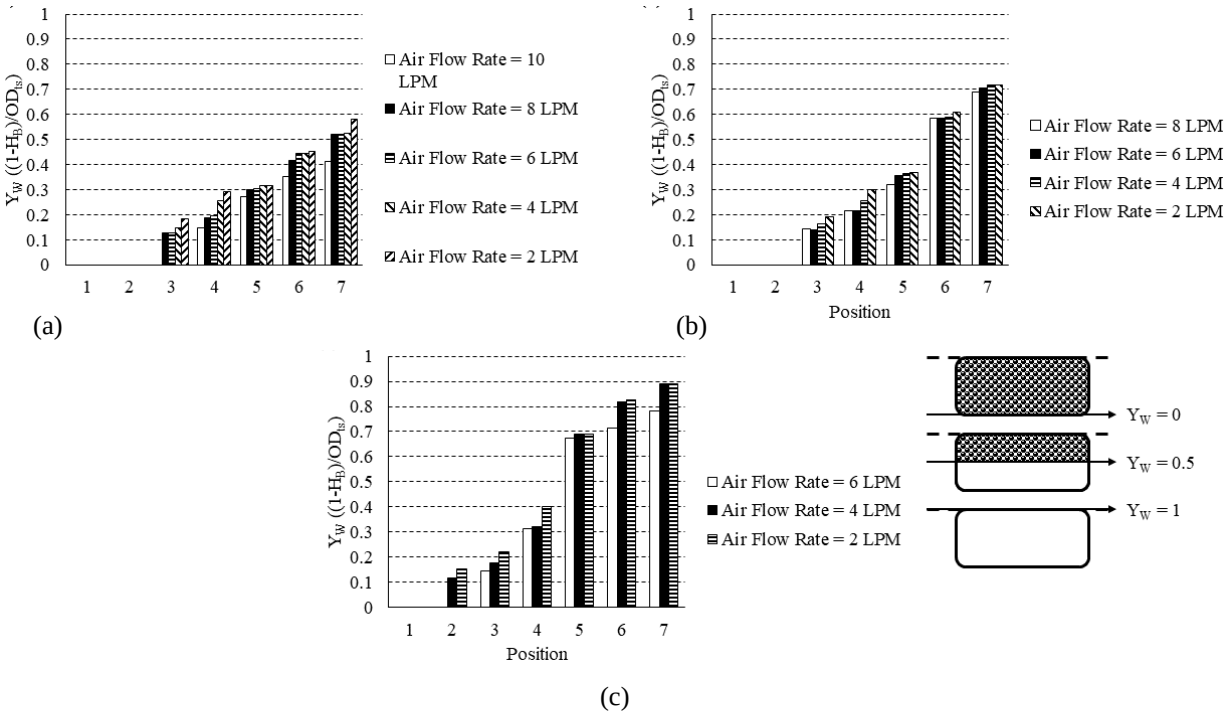

Fig. 8 Dimensionless parameter, Y_W for different Q_a at Q_w of (a) 170 LPM, (b) 145 LPM, and (c) 120 LPM

case. The Y_W from Position 1-7 for every case increases with decreasing Q_a from 10-2 LPM, which coincides with the findings from Fig. 8.

Lastly, several important findings in section 3.1 are summarized here. Table 5 shows that the overall bubble diameters from inlet to outlet of the horizontal tube (i.e., Position 1 to 7) decrease with decreasing Q_a. However, this finding is statistically insignificant ($p > 0.001$), indicating that Q_a is not a significant factor affecting bubble size. The bubble diameters at constant Q_w increase axially from Position 1-7 due to bubble coalescence and show about linear relationship with the axial position; This result is statistically significant ($p < 0.001$). The standard deviations of bubble diameters at Position 1-4 are smaller compared to Position 5-7 because of the lower tendency of bubble coalescence due to it being located nearer to the inlet of horizontal tube. The increase in bubble diameters from Position 1-7 increases with increasing Q_a at Q_w of 170 LPM and 145 LPM due to the increasing tendency of bubble coalescence but decreases with increasing Q_a at Q_w of 120 LPM. The changes in α with the axial position are statistically insignificant ($p > 0.001$). The Y_W increases with the axial position. The Y_W also increases with decreasing Q_a due to the reduced velocity of bubbles.

3.2 The Effects of Q_w

The diameters of bubbles for Q_w of 120-170 LPM at constant Q_a of 6 LPM are presented in box plots, see Fig. 9. By comparing the bubble diameters at Q_w of 120-170 LPM from inlet to outlet of the horizontal tube (i.e., Position 1 to 7), the changes in bubble diameters with varying Q_w at all axial positions are minimal and insignificant. Now compare the bubble sizes between Position 1-4 (near inlet) and Position 5-7 (near outlet). The standard deviations of bubble diameters at Position 1-4 are smaller in comparison with that of Position 5-7. For example, referring to Fig. 9a and Fig. 9e, the distribution of bubble diameters at Position 1 is smaller compared to Position 5. These two findings coincide with the results for constant Q_w in section 3.1.

The overall bubble diameters for varying Q_w are tabulated in Table 6. The asterisk symbols within the p-value column indicate that the changes in bubble diameters with different Q_w are statistically significant ($p < 0.001$). There are a total of 28 data sets with 20-30 data taken for each set (10 bubbles for each Q_w). The overall bubble diameters increase from inlet to outlet of the horizontal tube (i.e., Position 1 to 7) at constant Q_a of 2 LPM, 4 LPM, 6 LPM and 8 LPM. The standard deviations of overall bubble diameters at Position 1-4 are also lower than that of Position 5-7. For example, referring to Position 1 and Position 5 at Q_a of 8 LPM, the overall bubble diameter at Position 1 is 1.477±0.291 mm, of which the standard deviation is smaller than Position 5 with an overall diameter of 3.604±0.811 mm. This finding agrees well with the results from Fig. 9. Statistical analyses show that 19 out of 28 data sets collected have $p > 0.001$, which means that Q_w is also not a significant factor that influences bubble size. However, 9 out of 28 data sets collected have $p < 0.001$, which are more than the number of data set collected from Table 4 that have $p < 0.001$. This could indicate that Q_w is more prone to affect bubble size compared to Q_a, as reported by Wang et al. (2020).

The bubble diameters from inlet to outlet of the horizontal tube (i.e., Position 1 to 7) at constant Q_a of 6 LPM are presented in box plots, see Fig. 10. The bubble diameters increase with the axial distance from Position 1-7; The increase appears to be linear with the axial position as well. Now compare the bubble sizes between Position 1-4 (near inlet) and Position 5-7 (near outlet). The standard

Table 5 Overall diameter of bubbles at different Q_w

Q_a (LPM)	Q_w (LPM)	Position	Overall Diameter (mm)	P-Value
8 LPM (8.22±0.43 LPM)	Case B2 (168.28±2.23 LPM), Case C1 (143.33±2.58 LPM)	1	1.477±0.291	> 0.001
		2	2.264±0.417	> 0.001
		3	2.608±0.591	> 0.001
		4	3.352±0.689	> 0.001
		5	3.604±0.811	> 0.001
		6	3.816±0.622	> 0.001
		7	3.851±0.73	> 0.001
6 LPM (6.02±0.42 LPM)	Case B3 (169.05±1.76 LPM), Case C2 (143.46±2.04 LPM), Case D1 (118.66±1.69 LPM)	1	1.851±0.545	< 0.001*
		2	2.336±0.536	< 0.001*
		3	2.936±0.841	< 0.001*
		4	2.995±0.807	< 0.001*
		5	3.493±0.692	> 0.001
		6	3.846±0.662	> 0.001
		7	3.847±0.873	> 0.001
4 LPM (4.14±0.22 LPM)	Case B4 (172.21±2.43 LPM), Case C3 (145.32±2.24 LPM), Case D2 (120.33±1.51 LPM)	1	1.759±0.44	< 0.001*
		2	2.263±0.499	< 0.001*
		3	2.973±0.774	< 0.001*
		4	3.164±0.744	< 0.001*
		5	3.221±0.514	< 0.001*
		6	3.534±0.687	> 0.001
		7	3.761±0.609	> 0.001
2 LPM (2.02±0.08 LPM)	Case B5 (175.92±2.44 LPM), Case C4 (150.47±2.44 LPM), Case D3 (125.37±1.90 LPM)	1	1.682±0.252	> 0.001
		2	2.414±0.391	> 0.001
		3	2.448±0.322	> 0.001
		4	2.786±0.551	> 0.001
		5	3.295±0.553	> 0.001
		6	3.111±0.647	> 0.001
		7	3.388±0.649	> 0.001

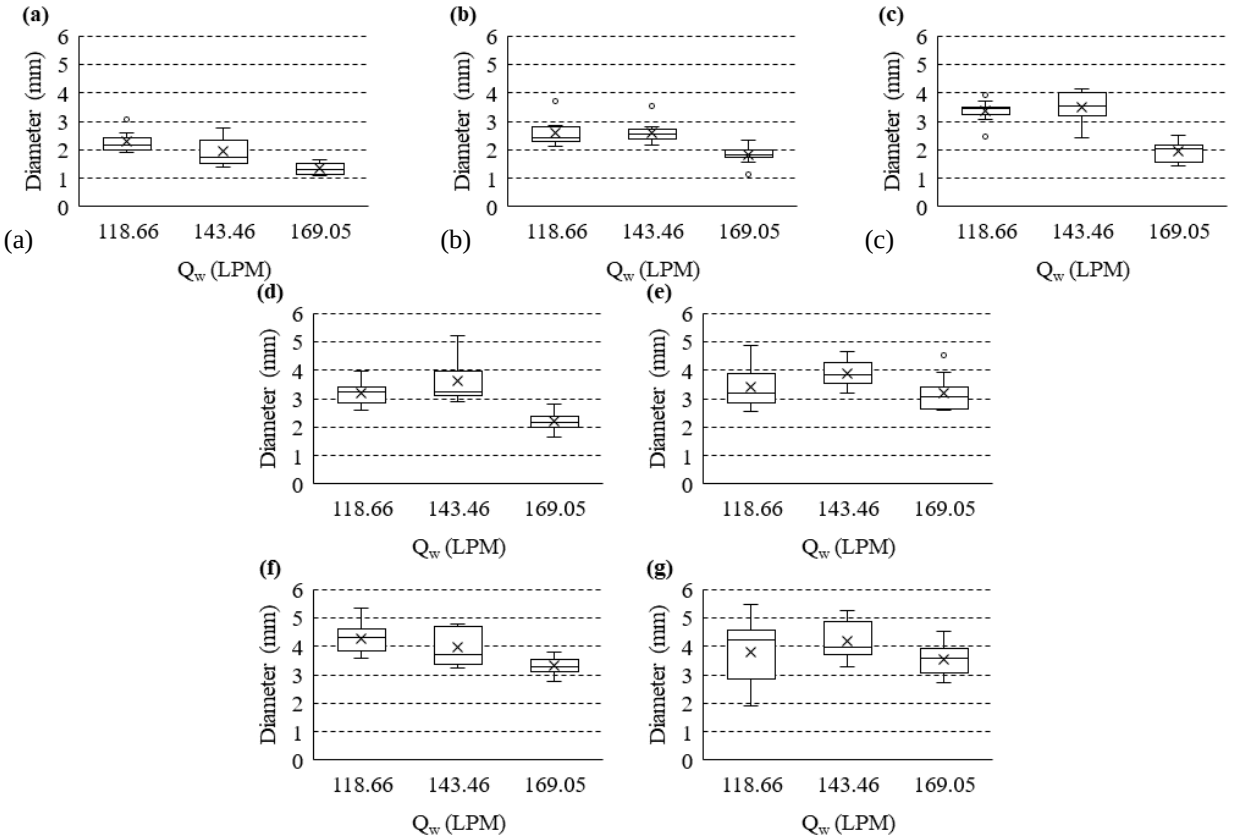

Fig. 9 Diameters of 10 bubbles at Position (a) 1, (b) 2, (c) 3, (d) 4, (e) 5, (f) 6, and (g) 7, for different Q_w at Q_a of 6 LPM

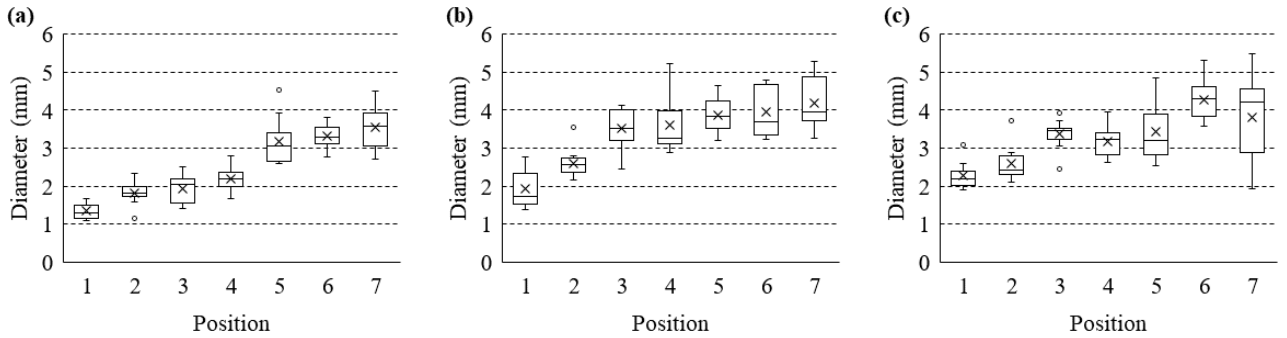

Fig. 10 Diameters of 10 bubbles at Q_a of 6 LPM with Q_w of (a) 170 LPM, (b) 145 LPM, and (c) 120 LPM

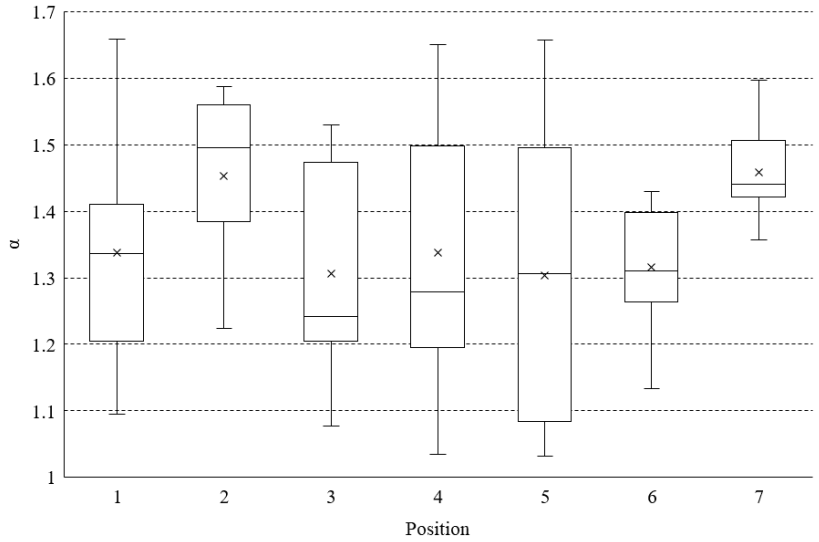

Fig. 11 Aspect ratios of 10 bubbles at Q_a of 6 LPM with Q_w of 145 LPM

deviations of bubble diameters at Position 1-4 are also smaller in comparison with that of Position 5-7. All these findings coincide with the results from Fig. 9 and Table 6, which have already been explained in section 3.1. Now refer to Table 5, the overall bubble diameters from Position 1-7 appear to be larger for lower Q_w. The finding of bubble diameter increases with decreasing Q_w has been reported by past literature (Li et al., 2017; Zhao et al., 2019; Wang et al., 2020; Ding et al., 2021; Sakamatapan et al., 2021). Note that the bubble size was evaluated directly in either the throat or divergence section of bubble generator in most past literature, whereas the bubble size was evaluated along a horizontal tube located 160 mm away from the bubble generator outlet in this study. The increase in bubble diameters from Position 1-7 seems to be larger for increasing Q_w; This is due to the increase in water velocity in the horizontal tube as Q_w increases, which increases the tendency of bubble coalescence. The aspect ratios of bubbles from inlet to outlet of the horizontal tube (i.e., Position 1 to 7) at Q_a of 6 LPM with Q_w of 145 LPM are presented in a box plot, see Fig. 11. The α varies within 1-1.7. The effect of the axial position on the α is statistically insignificant ($p > 0.001$) as well, which coincides with the finding from Fig. 6.

The Y_W from inlet to outlet of the horizontal tube (i.e., Position 1 to 7) at constant Q_a of 2 LPM is presented in a bar graph, see Fig. 10. The Y_W also increases axially from Position 1-7. At a fixed Q_a of 2 LPM, the Y_W increases with decreasing Q_w from 170-120 LPM. This is because the bubble diameter increases with decreasing Q_w, see Table 5. Hence, the rise velocity of bubbles increases with decreasing Q_w. Now refer to Position 5-7 at Q_w of 145 LPM and 120 LPM, the Y_W shows a dramatic increase when Q_w is reduced from 145 LPM to 120 LPM. This could indicate that Y_W is more sensitively affected by the change in Q_w compared to Q_a, just as the bubble size is more sensitive to the change in Q_w than Q_a. The results of Y_W at constant Q_a of 4 LPM, 6 LPM, and 8 LPM are similar, hence they are not shown here. Now refer to Table 5, the Y_W from Position 1-7 increases with decreasing Q_w, which agrees well with the results from Fig. 10.

Lastly, several important findings in section 3.2 are summarized here. Table 5 shows that the overall bubble diameters from inlet to outlet of the horizontal tube (i.e., Position 1 to 7) decrease with decreasing Q_w. This finding is statistically insignificant ($p > 0.001$), which indicates that Q_w is not a significant factor in affecting bubble size as well. However, by comparing the p-values in Table 4 and Table 6, the bubble size is more sensitively affected by Q_w compared to Q_a. The bubble diameters at constant Q_a increase axially from Position 1-7 due to bubble coalescence and show about linear relationship with the

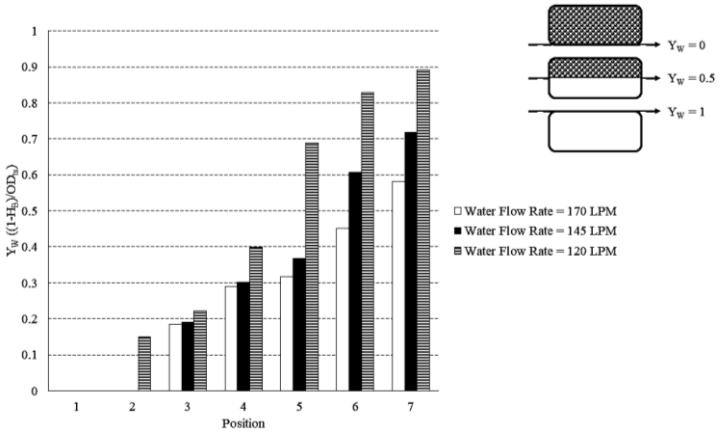

Fig. 12 Dimensionless parameter, Y_W for different Q_w at Q_a of 2 LPM

axial position (same finding as varying Q_a). This result is statistically significant ($p < 0.001$). The standard deviations of bubble diameters at Position 1-4 are smaller compared to Position 5-7 because of the lower probability of bubble coalescence due to it being located nearer to the inlet of horizontal tube (same finding as varying Q_a). The increase in bubble diameters from Position 1-7 increases with increasing Q_w. The changes in α with the axial position are statistically insignificant ($p > 0.001$) as well. The Y_W increases with the axial position (same finding as varying Q_a). The Y_W also increases with decreasing Q_w due to the increased rise velocity of bubbles. Q_w is a more prominent factor compared to Q_a in affecting the Y_W.

3.3 Characterization of Bubble Size using Weber Number

Weber number (We) is a dimensionless number that characterizes bubble deformation using the ratio of inertial force on a bubble to surface tension force on the bubble. The We used to characterize the bubble size in this study is defined in Eq. (4).

$$We_m = \frac{\rho_w V_w{}^2 D_m}{\sigma} \tag{4}$$

Where We_m is the mean Weber number, ρ_w is the density of water, V_w is the velocity of water in the horizontal tube, D_m is the mean equivalent diameters of the 10 bubbles, and σ is the surface tension of water-air interface. From Eq. (4), it is clear that the Weber number is dependent on the velocity of liquid, properties of fluids, and diameter of bubbles. The We_m along the horizontal tube at 120 LPM≤Q_w≤170 LPM and 2 LPM≤Q_a≤10 LPM is displayed in Fig. 13. From Fig. 13, it can be observed that the We_m along the horizontal tube for Q_a of 2-10 LPM at Q_w of 170 LPM, 145 LPM, and 120 LPM are within 80-250, 60-200, and 60-140, respectively. The We_m increases from inlet to outlet of the horizontal tube (i.e., Position 1 to 7) because of the increase in bubble size due to bubble coalescence. Besides, the We_m at all Q_a decreases when Q_w decreases due to the reduced velocity of water in the horizontal tube; The decrease in We_m is more significant at Position 5-7 compared to Position 1-4 at all Q_a.

3.4 Multiphase Flow Regime

The flow pattern map for gas-liquid flow in horizontal pipes by Mandhane et al. (1974) is shown in Fig. 14. The

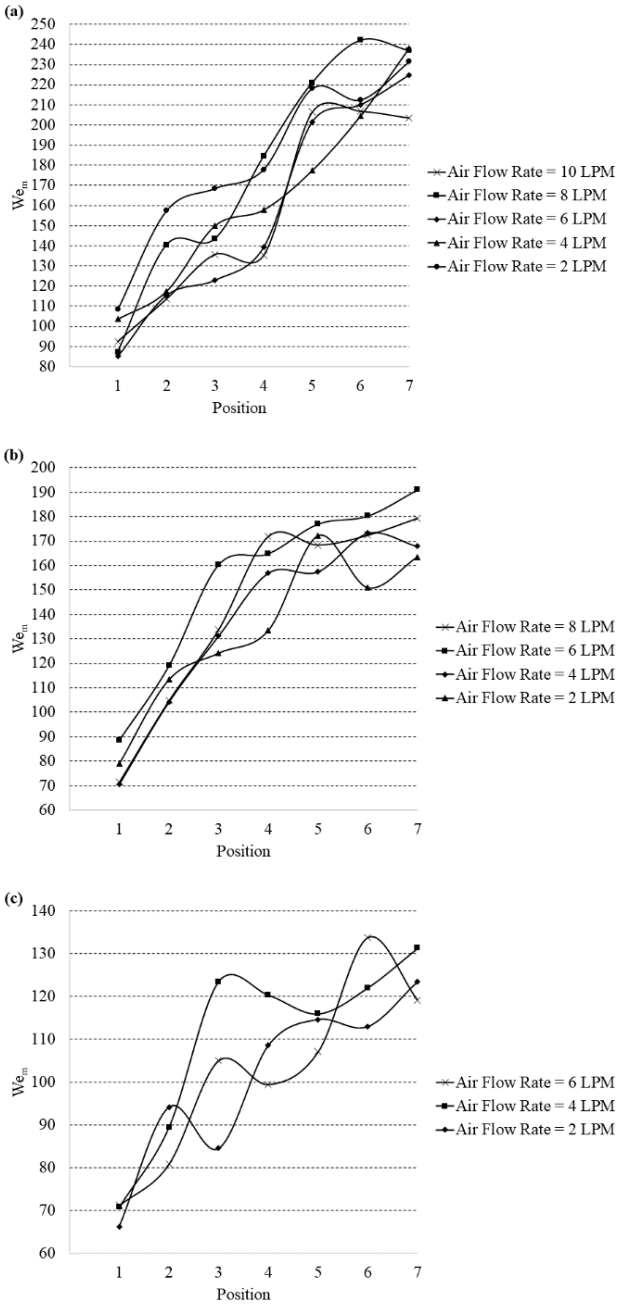

Fig. 13 Mean Weber number along horizontal tube for different Qa at Qw of (a) 170 LPM, (b) 145 LPM, and (c) 120 LPM

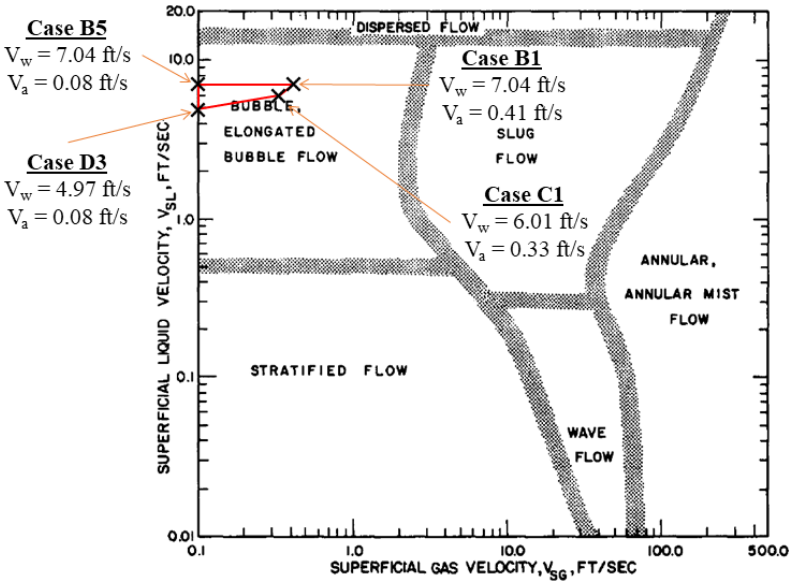

Fig. 14 Flow pattern map for gas-liquid flow in horizontal pipes (Mandhane et al. 1974)

experimental range of Q_w and Q_a in this study are plotted in Fig. 13. It is assumed that the volumetric flow-rate of air bubbles in the horizontal tube is equal to Q_a, which is the air flow-rate measured at the air inlet of the venturi-nozzle bubble generator. From Fig. 14, it is easily observed that 120 LPM≤Q_w≤170 LPM and 2 LPM≤Q_a≤10 LPM are within the regime of bubble/elongated bubble flow, which is consistent with our observations during the experiments. The Lockhart-Martinelli parameter is used to define the relationship between the densities of components in a two-phase flow and their mass flow rates analytically (Liu et al., 2020). The Lockhart-Martinelli parameter is defined in Eq. (5) (Carvajal et al., 2018).

$$\chi = \frac{Q_l}{Q_g}\sqrt{\frac{\rho_g}{\rho_l}} \tag{5}$$

Where χ is the Lockhart-Martinelli parameter, Q_l is the volumetric flow-rate of the liquid, Q_g is the volumetric flow-rate of the gas, ρ_g is the volumetric flow-rate of the gas, and ρ_l is the volumetric flow-rate of the liquid. The χ for all the cases are tabulated in Table 7. Liu et al. (2020) stated that the two-phase flow is identified as wet gas flow and multiphase flow when $\chi \leqslant 0.3$ and $\chi > 0.3$, respectively. From Table 7, the χ for all the experimental cases in this study are within 0.58-2.94. This indicates that the two-phase flow in the horizontal tube is a multiphase flow (bubble flow), which agrees well with our observations during the experiments.

4. CONCLUSION

The flow of bubbles produced by venturi-nozzle bubble generator at 120 LPM≤Q_w≤170 LPM and 2 LPM≤Q_a≤10 LPM were captured along a horizontal tube (test section) using high-speed camera. The bubble size, which is defined by bubble equivalent diameter, was evaluated using MATLAB. Note that the bubble size was evaluated directly in either the throat or divergence section of bubble generator in most past literature, whereas the bubble size was evaluated along a horizontal tube located

Table 7 Lockhart-Martinelli parameter for all the experimental cases

Case	Q_w (LPM)	Q_a (LPM)	χ
B1	167.24	9.83	0.58
B2	168.28	8.16	0.70
B3	169.05	6.15	0.94
B4	172.21	4.19	1.40
B5	175.92	2.04	2.94
C1	143.33	8.27	0.59
C2	143.46	6.03	0.81
C3	145.32	4.08	1.22
C4	150.47	2.01	2.56
D1	118.66	5.89	0.69
D2	120.33	4.19	0.98
D3	125.37	2.02	2.12

160 mm away from the bubble generator outlet in this study. The vertical rise height of bubbles, which is defined by the Y_W dimensionless parameter, along a horizontal tube was evaluated as well. In addition, the bubble size along the horizontal tube was characterized by the mean Weber number (We_m). Lastly, the type of two-phase (water-air bubbles) flow in the horizontal tube was determined using flow pattern map and Lockhart-Martinelli parameter. In this study, the effects of two operating conditions, which are Q_a and Q_w on the bubbles generated by the bubble generator were investigated experimentally. The following are the main findings obtained from this study:

- The bubble generator produces bubbles with diameters of 0.8-3.1 mm at the inlet of horizontal tube (Position 1).
- The bubble diameters at either constant Q_w or Q_a increase axially from inlet to outlet of the horizontal tube (i.e., Position 1 to 7) due to bubble coalescence and show about linear relationship with the axial position. The results are statistically significant ($p < 0.001$).

- The standard deviations of bubble diameters at Position 5-7 are higher compared to Position 1-4 because of the higher tendency of bubble coalescence due to being located nearer to the outlet of horizontal tube.
- The increase in bubble diameters from Position 1-7 increases with either increasing Q_a or Q_w (except for increasing Q_a at Q_w of 120 LPM) due to the increasing tendency of bubble coalescence.
- Q_a and Q_w have no significant effect on the bubble diameters. However, the bubble diameters are more sensitive to the change in Q_w than Q_a.
- The changes in bubble aspect ratio (α) with the axial position are statistically insignificant ($p > 0.001$).
- The vertical rise height of bubbles (Y_W) increases axially from Position 1-7.
- The Y_W increases when either the Q_a or Q_w is reduced due to the reduced velocity of bubbles and increased rise velocity of bubbles, respectively. However, the Y_W is more sensitive to the change in Q_w than Q_a.
- The mean Weber number (We_m) increases from Position 1-7 because of the increase in bubble size due to bubble coalescence.
- The decrease in Q_w reduces the water velocity in the horizontal tube, thus decreasing the We_m at all Q_a. The decrease in We_m due to the decrease in Q_w is more pronounced at Position 5-7 compared to Position 1-4 at all Q_a.
- The Lockhart-Martinelli parameters are within 0.58-2.94, which indicates that the two-phase (water-air bubbles) flow in the horizontal tube is a multiphase flow.

However, there were two major experiment limitations in this study. The first limitation was that the maximum achievable Q_a by the venturi-nozzle bubble generator was only around 10 LPM. This was because air compressor was not used during the experiments. The bubble generator only utilized passive (vacuum) air suction to produce air bubbles. The maximum Q_a that is achievable by venturi-nozzle bubble generator through passive air suction is highly dependent on its internal geometrical design. The second limitation was that the maximum Q_w by the water pump was only around 170 LPM. This was because the Q_w was limited by the input power of the water pump, which was only 0.25 kW. The specified water pump was used during the experiments because it was capable of recirculating 5,000-10,000 litre of water in a water tank for aquaculture application, which was the main motivation of this study.

ACKNOWLEDGEMENTS

This study was funded by Universiti Malaya Impact-oriented Interdisciplinary Research Grant (IIRG005A-2020IISS).

CONFLICT OF INTEREST

The authors have no competing interests or conflicts to disclose.

AVAILABILITY OF DATA AND MATERIALS

The data that support the findings of this study are available from the corresponding author upon reasonable request.

AUTHORS CONTRIBUTION

Goo Wei Hong: Conceptualization; methodology; formal analysis; writing – original draft; Poo Balan Ganesan: Conceptualization; funding acquisition; supervision; methodology; resources; visualization; writing – review & editing; Yong Kok Wee: Visualization; writing – review and editing; Mohd Yazed Ahmad: Supervision; Yau Yat Huang: Supervision; Faik Hamad: Methodology.

REFERENCES

Baylar, A., & Ozkan, F. (2006). Applications of venturi principle to water aeration systems. *Environmental Fluid Mechanics*, 6(4), 341-357. https://doi.org/10.1007/s10652-005-5664-9

Boyd, C. E. (1998). Pond water aeration systems. *Aquacultural engineering*, 18(1), 9-40. https://doi.org/10.1016/S0144-8609(98)00019-3

Carvajal, G., Maucec, M., & Cullick, S. (2018). *Intelligent digital oil and gas fields: Concepts, collaboration, and right-time decisions*. Gulf Professional Publishing. https://doi.org/10.1016/B978-0-12-804642-5.00002-5

Ding, G., Chen, J., Li, Z., Cai, X., & Ji, Y. (2022). An investigation on the bubbly flow of a Venturi channel based on the population balance model. *The Canadian Journal of Chemical Engineering*, 100(7), 1652-1664. https://doi.org/10.1002/cjce.24258

Ding, G., Li, Z., Chen, J., & Cai, X. (2021). An investigation on the bubble transportation of a two-stage series venturi bubble generator. *Chemical Engineering Research and Design*, 174, 345-356. https://doi.org/10.1016/j.cherd.2021.08.022

Gordiychuk, A., Svanera, M., Benini, S., & Poesio, P. (2016). Size distribution and Sauter mean diameter of micro bubbles for a Venturi type bubble generator. *Experimental Thermal and Fluid Science*, 70, 51-60. https://doi.org/10.1016/j.expthermflusci.2015.08.014

Huang, J., Sun, L., Du, M., Liang, Z., Mo, Z., Tang, J., & Xie, G. (2020). An investigation on the performance of a micro-scale Venturi bubble generator. *Chemical engineering journal*, 386, 120980. https://doi.org/10.1016/j.cej.2019.02.068

Huang, J., Sun, L., Du, M., Mo, Z., & Zhao, L. (2018). A visualized study of interfacial behavior of air–water

two-phase flow in a rectangular Venturi channel. *Theoretical and Applied Mechanics Letters*, 8(5), 334-344. https://doi.org/10.1016/j.taml.2018.05.004

Huang, J., Sun, L., Mo, Z., Feng, Y., Bao, J., & Tang, J. (2021). Experimental investigation on the effect of throat size on bubble transportation and breakup in small Venturi channels. *International Journal of Multiphase Flow*, 142, 103737. https://doi.org/10.1016/j.ijmultiphaseflow.2021.103737

Huang, J., Sun, L., Mo, Z., Liu, H., Du, M., Tang, J., & Bao, J. (2019). A visualized study of bubble breakup in small rectangular Venturi channels. *Experimental and Computational Multiphase Flow*, 1(3), 177-185. https://doi.org/10.1007/s42757-019-0018-x

Kurata, K., Taniguchi, H., Fukunaga, T., Matsuda, J., & Higaki, H. (2007). Development of a compact microbubble generator and its usefulness for three-dimensional osteoblastic cell culture. *Journal of Biomechanical Science and Engineering*, 2(4), 166-177. https://doi.org/10.1299/jbse.2.166

Lee, C. H., Wongwises, S., Jerng, D. W., & Ahn, H. S. (2021). Experimental study on breakup mechanism of microbubble in 2D channel. *Case Studies in Thermal Engineering*, 28, 101523. https://doi.org/10.1016/j.csite.2021.101523

Levitsky, I., Tavor, D., & Erenburg, V. (2022). A new bubble generator for creation of large quantity of bubbles with controlled diameters. *Experimental and Computational Multiphase Flow*, 4(1), 45-51. https://doi.org/10.1007/s42757-020-0085-z

Li, J., Song, Y., Yin, J., & Wang, D. (2017). Investigation on the effect of geometrical parameters on the performance of a venturi type bubble generator. *Nuclear Engineering and Design*, 325, 90-96. https://doi.org/10.1016/j.nucengdes.2017.10.006

Liu, X., Lao, L., & Falcone, G. (2020). A comprehensive assessment of correlations for two-phase flow through Venturi tubes. *Journal of Natural Gas Science and Engineering*, 78, 103323. https://doi.org/10.1016/j.jngse.2020.103323

Liu, Y., Zhou, Y., Wang, T., Pan, J., Zhou, B., Muhammad, T., Zhou, C., & Li, Y. (2019). Micro-nano bubble water oxygation: Synergistically improving irrigation water use efficiency, crop yield and quality. *Journal of Cleaner Production*, 222, 835-843. https://doi.org/10.1016/j.jclepro.2019.02.208

Mandhane, J., Gregory, G., & Aziz, K. (1974). A flow pattern map for gas—liquid flow in horizontal pipes. *International Journal of Multiphase Flow*, 1(4), 537-553. https://doi.org/10.1016/0301-9322(74)90006-8

Murai, Y., Tasaka, Y., Oishi, Y., & Ern, P. (2021). Bubble fragmentation dynamics in a subsonic Venturi tube for the design of a compact microbubble generator. *International Journal of Multiphase Flow*, 139, 103645. https://doi.org/10.1016/j.ijmultiphaseflow.2021.103645

Roy, S. M., Machavaram, R., Pareek, C., & Mal, B. (2021). Diversified aeration facilities for effective aquaculture systems—a comprehensive review. *Aquaculture International*, 29(3), 1181-1217. https://doi.org/10.1007/s10499-021-00685-7

Sadatomi, M., Kawahara, A., Kano, K., & Ohtomo, A. (2005). Performance of a new micro-bubble generator with a spherical body in a flowing water tube. *Experimental Thermal and Fluid Science*, 29(5), 615-623. https://doi.org/10.1016/j.expthermflusci.2004.08.006

Sadatomi, M., Kawahara, A., Matsuura, H., & Shikatani, S. (2012). Micro-bubble generation rate and bubble dissolution rate into water by a simple multi-fluid mixer with orifice and porous tube. *Experimental Thermal and Fluid Science*, 41, 23-30. https://doi.org/10.1016/j.expthermflusci.2012.03.002

Sakamatapan, K., Mesgarpour, M., Mahian, O., Ahn, H. S., & Wongwises, S. (2021). Experimental investigation of the microbubble generation using a venturi-type bubble generator. *Case Studies in Thermal Engineering*, 27, 101238. https://doi.org/10.1016/j.csite.2021.101238

Song, Y., Wang, D., Yin, J., Li, J., & Cai, K. (2019). Experimental studies on bubble breakup mechanism in a venturi bubble generator. *Annals of Nuclear Energy*, 130, 259-270. https://doi.org/10.1016/j.anucene.2019.02.020

Sun, L., Mo, Z., Zhao, L., Liu, H., Guo, X., Ju, X., & Bao, J. (2017). Characteristics and mechanism of bubble breakup in a bubble generator developed for a small TMSR. *Annals of Nuclear Energy*, 109, 69-81. https://doi.org/10.1016/j.anucene.2017.05.015

Terasaka, K., Hirabayashi, A., Nishino, T., Fujioka, S., & Kobayashi, D. (2011). Development of microbubble aerator for waste water treatment using aerobic activated sludge. *Chemical Engineering Science*, 66(14), 3172-3179. https://doi.org/10.1016/j.ces.2011.02.043

Verma, A. K., Bhunia, P., Dash, R. R., Tyagi, R. D., Surampalli, R. Y., & Zhang, T. C. (2015). Effects of physico-chemical pre-treatment on the performance of an upflow anaerobic sludge blanket (UASB) reactor treating textile wastewater: application of full factorial central composite design. *The Canadian Journal of Chemical Engineering*, 93(5), 808-818. https://doi.org/10.1002/cjce.22168

Wang, X., Shuai, Y., Zhang, H., Sun, J., Yang, Y., Huang, Z., Jiang, B., Liao, Z., Wang, J., & Yang, Y. (2021). Bubble breakup in a swirl-venturi microbubble generator. *Chemical Engineering Journal*, 403, 126397. https://doi.org/10.1016/j.cej.2020.126397

Wang, X., Shuai, Y., Zhou, X., Huang, Z., Yang, Y., Sun, J., Zhang, H., Wang, J., & Yang, Y. (2020).

Performance comparison of swirl-venturi bubble generator and conventional venturi bubble generator. *Chemical Engineering and Processing-Process Intensification*, 154, 108022. https://doi.org/10.1016/j.cep.2020.108022

Wilson, D. A., Pun, K., Ganesan, P. B., & Hamad, F. (2021). Geometrical optimization of a venturi-type microbubble generator using CFD simulation and experimental measurements. *Designs*, 5(1), 4. https://doi.org/10.3390/designs5010004

Yin, J., Li, J., Li, H., Liu, W., & Wang, D. (2015). Experimental study on the bubble generation characteristics for an venturi type bubble generator. *International Journal of Heat and Mass Transfer*, 91, 218-224. https://doi.org/10.1016/j.ijheatmasstransfer.2015.05.076

Yun, J. E., & Kim, J. H. (2014). Development of venturi system for microbubble generation. *Transactions of the Korean Society of Mechanical Engineers B*, 38(10), 865-871. https://doi.org/10.3795/KSME-B.2014.38.10.865

Zhang, L., Liu, J., Liu, C., Zhang, J., & Yang, J. (2016). Performance of a fixed-bed biofilm reactor with microbubble aeration in aerobic wastewater treatment. *Water Science and Technology*, 74(1), 138-146. https://doi.org/10.2166/wst.2016.187

Zhao, L., Mo, Z., Sun, L., Xie, G., Liu, H., Du, M., & Tang, J. (2017). A visualized study of the motion of individual bubbles in a venturi-type bubble generator. *Progress in Nuclear Energy*, 97, 74-89. https://doi.org/10.1016/j.pnucene.2017.01.004

Zhao, L., Sun, L., Mo, Z., Du, M., Huang, J., Bao, J., Tang, J., & Xie, G. (2019). Effects of the divergent angle on bubble transportation in a rectangular Venturi channel and its performance in producing fine bubbles. *International Journal of Multiphase Flow*, 114, 192-206. https://doi.org/10.1016/j.ijmultiphaseflow.2019.02.003

Zhao, L., Sun, L., Mo, Z., Tang, J., Hu, L., & Bao, J. (2018). An investigation on bubble motion in liquid flowing through a rectangular Venturi channel. *Experimental Thermal and Fluid Science*, 97, 48-58. https://doi.org/10.1016/j.expthermflusci.2018.04.009